

# Regulating triacylglycerol cycling for high-efficiency production of polyunsaturated fatty acids and derivatives

Received: 9 January 2025

Accepted: 29 April 2025

Published online: 08 May 2025

Fei Du<sup>1,2,3</sup>, Qing Xu<sup>1,2,3</sup>, Xin Li<sup>2</sup>, Yiwen Hang<sup>2</sup>, Duoduo Zhang<sup>2</sup>, Feng Zhang<sup>2</sup>, Wang Ma<sup>2</sup>, Xiaoman Sun<sup>1,2</sup>  & He Huang<sup>1,2</sup> 

Lipid degradation is generally considered an antagonistic pathway to lipid synthesis, so this pathway is often removed to improve lipid production. In this study, triacylglycerol (TAG) cycling formed by lipid degradation is found to be crucial for long-chain polyunsaturated fatty acid (PUFA) biosynthesis; this result contradicts the notion that lipid degradation is a useless process. Specifically, we demonstrate that TAG cycling promoting PUFA biosynthesis occurred in *Yarrowia lipolytica* and *Mortierella alpina* via the desaturase/elongase pathway but not in *Schizochytrium* sp. with the polyketide synthase (PKS) pathway. Exploiting the TAG cycling mechanism, a strategy of decoupling the TAG biosynthesis and degradation is developed. Using this strategy, the titers of C20:5, C22:5 and prostaglandin F2 $\alpha$  (PGF2 $\alpha$ ) in *Y. lipolytica* are improved by 116.2%, 99.4% and 41.7%, respectively. Our findings highlight the potential of the TAG cycling for related biochemical synthesis in the construction of excellent oleaginous engineered strains.

Microbial lipids have attracted considerable interest owing to their green and efficient production methods<sup>1,2</sup>. Owing to their fatty acid (FA) composition, microbial lipids can be used as promising sources of next-generation biodiesel or food additives and pharmaceuticals<sup>3,4</sup>. Accordingly, increased research interest has focused on genetic and metabolic engineering approaches to construct engineered oleaginous cell factories for storing and producing large amounts of lipids with an attractive FA composition<sup>5–7</sup>. Microbial lipids are primarily composed of triacylglycerol (TAG). In general, TAG is synthesized by a variety of acyltransferases using free FAs and glycerol as substrates, and this process follows the Kennedy pathway<sup>8</sup>. Moreover, TAG can be hydrolyzed by lipase to release free FAs and glycerol, then esterified FAs can be recycled into other lipids or degraded via  $\beta$ -oxidation to provide metabolic energy for cellular maintenance<sup>9</sup>. Blocking the TAG degradation pathway has become a promising strategy in constructing efficient lipid-producing cell factories, such as abolishing the  $\beta$ -oxidation pathway or lipase<sup>10</sup>, and studies showed that the lipid titer can be increased by 2.0–4.6 times using the strategy<sup>11,12</sup>. Accordingly,

TAG degradation is considered a futile process in constructing a superior cell factory for lipid production.

The process of continuous degradation and resynthesis of TAG is called TAG cycling<sup>13</sup>. In recent years, emerging evidence has indicated that TAG cycling plays important roles in systemic metabolic homeostasis<sup>14</sup>. For example, FAs for membrane lipid synthesis are derived mainly from TAG degradation rather than de novo biosynthesis via the fatty acid synthesis pathway; this demonstrates the importance of TAG degradation for supporting efficient growth initiation<sup>15,16</sup>. TAG cycling could also moderate the oxidation rate of FA by calibrating the availability of acyl-CoAs, and then further impact the intracellular acetyl-CoA concentration and redox homeostasis<sup>17</sup>. Importantly, a recent study demonstrated that TAG cycling might provide a window for lipid diversification. The FAs released from TAG cycling could be modified by elongation and desaturation such that saturated FAs could be converted to monounsaturated FAs in preadipocytes<sup>18</sup>. Therefore, considering the importance of TAG cycling, the ability of blocking the TAG degradation pathway to

<sup>1</sup>State Key Laboratory of Microbial Technology, Nanjing Normal University, Nanjing, People's Republic of China. <sup>2</sup>School of Food Science and Pharmaceutical Engineering, Nanjing Normal University, Nanjing, People's Republic of China. <sup>3</sup>These authors contributed equally: Fei Du, Qing Xu.

 e-mail: [xiaomansun@njnu.edu.cn](mailto:xiaomansun@njnu.edu.cn)

increase the lipid titer of oleaginous microorganisms may need to be revised.

In this study, by exploring the changes of the FA profiles in three industrial oleaginous microorganisms (*Yarrowia lipolytica*, *Schizochytrium* sp., and *Mortierella alpina*), five putative mechanisms for TAG cycling are proposed and examined. We demonstrate that, based on the desaturase/elongase pathway, TAG cycling facilitates the conversion of saturated FAs to long-chain polyunsaturated fatty acids (PUFAs) with prolonged fermentation time. Exploiting this TAG cycling mechanism, we develop a strategy that TAG biosynthesis and degradation are decoupled to increase the production of PUFAs and their derivatives. As a proof of concept, the production of C20:5, C22:5, and prostaglandin F<sub>2</sub> $\alpha$  (PGF<sub>2</sub> $\alpha$ ) is examined. Our findings highlight the important role of lipid degradation in the construction of excellent oleaginous engineered strains.

## Results

### FA profile in different microorganisms under fed-batch fermentation

Three PUFA producers (engineered *Y. lipolytica* YIP56 for C20:5, *Schizochytrium* sp. for C22:6, and *M. alpina* for C20:4) were used to explore the differences in their FA profile changes. In particular, PUFAs were biosynthesized by the desaturase/elongase pathway in *Y. lipolytica* and *M. alpina* (Fig. 1a)<sup>19</sup>, whereas PUFAs were biosynthesized by the polyketide synthase (PKS) pathway in *Schizochytrium* sp. (Fig. 1b)<sup>20</sup>. As shown in Fig. 1c, the C16 and C18 FA contents (% total fatty acids, TFAs) of *Y. lipolytica* YIP56 continuously decreased with prolonged fermentation time. The contents of C16:0 and C18:2 significantly decreased from 28.4% and 34.8% at 48 h to 9.24% and 10.4% at 240 h, respectively. The content of C20:5 continuously increased, and the final content reached 40.5% at 240 h (Fig. 1c). The variation in the FA content of *M. alpina* R807 was similar to that of *Y. lipolytica*. The contents of C16:0 and C18:1 decreased from 18.6% and 21.7% at 48 h to 12.4% and 11.5% at 240 h, respectively, whereas the content of C20:4 continuously

increased, and the final content reached 46.2% at 240 h (Fig. 1d). However, the FA profile of *Schizochytrium* sp. HX308 exhibited the opposite trend during fermentation. After 120 h, the contents of C14:0 and C16:0 continued to increase, whereas the content of C22:6 decreased from 48.7% at 120 h to 32.5% at 192 h (Fig. 1e). Moreover, the lipid titer and dry cell weight (DCW) of the three producers decreased at the later stage of fermentation (Supplementary Fig. 1a–c). For example, the lipid titer of the YIP56 strain decreased by 30.2%, from 31.8 g/L at 192 h to 22.2 g/L at 240 h; these results indicated that lipids were degraded at the later stage of fermentation.

### Identifying the potential lipid species for the FA profile changes

To explore whether the increase of C20:5 content accompanied with the decrease of lipid titer was related to the difference in lipid species, lipidomics at eight time points in *Y. lipolytica* YIP56 was tested and analyzed (Fig. 2a). The final analysis covered seven lipid species of the YIP56 strain, including TAG, diacylglycerol (DAG), monoacylglyceride (MAG), phosphatidic acid (PA), phosphatidylcholine (PC), phosphatidylethanolamine (PE), and phosphatidylinositol (PI). As shown in Fig. 2b, c, with prolonged fermentation time, the contents of C16:0 and C18:2 gradually decreased in TAG (Fig. 2b) and DAG (Fig. 2c), whereas the contents of C20:5 gradually increased. Similarly, the content of C20:5 in MAG continuously increased (Fig. 2d); thus, there was more esterified C20:5 than C16:0 and C18:2 on MAG molecule, which might indicate that endogenous lysophosphatidate acyl-transferase (LPAAT), which catalyzes sn-2 position of the TAG molecules, has high substrate preference for C20:5-CoA. In addition, PC, PE, PA and PI are the major phospholipid components in *Y. lipolytica*, which accounts for 0.7–4.2% in total lipids (Supplementary Fig. 2). There is a decrease in C20:5 content was observed in the PE and PA in the later fermentation stage, and although PC and PI are different from them, their low level was not sufficient to cause an increase in C20:5 content in Fig. 1c (Fig. 2e–h).

In *Y. lipolytica*, TAG was the main species involved in lipid storage and accounted for 70% of the total lipids; this was followed by DAG

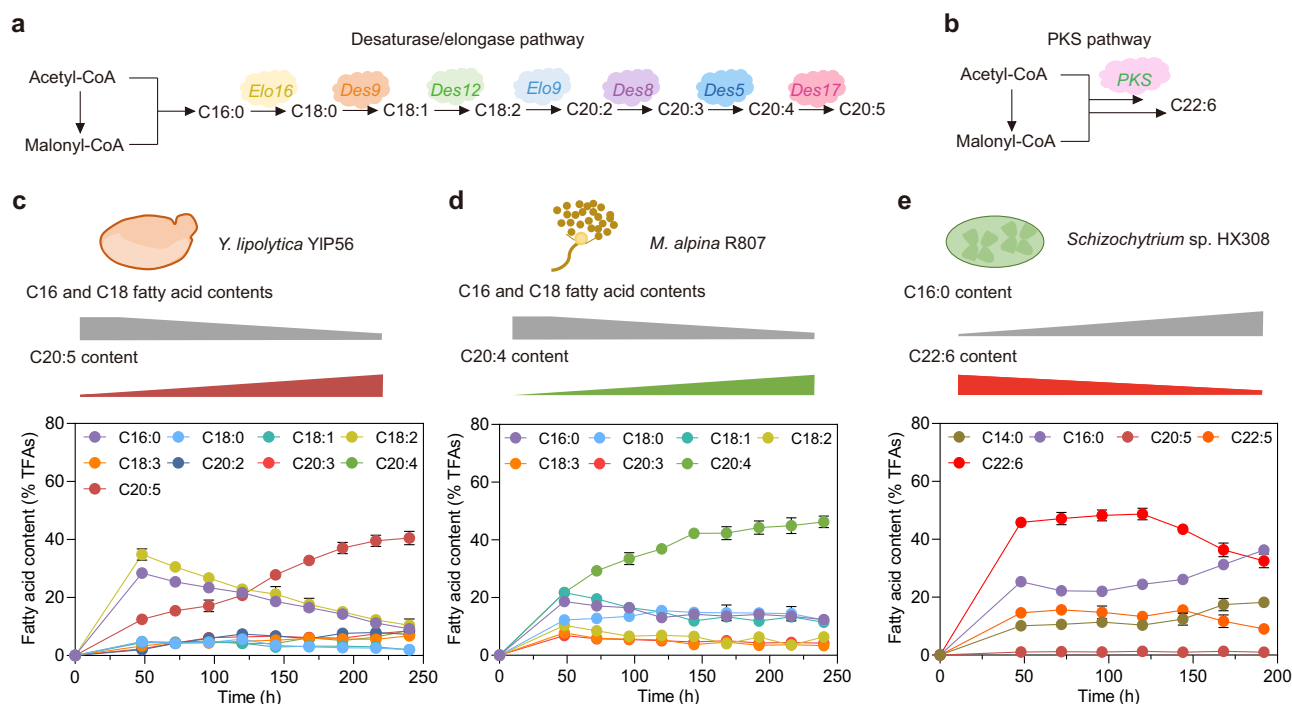


**Fig. 1 | Analysis of fatty acid profiles in three microorganisms under fed-batch fermentation.** **a** Desaturase/elongase pathway. *Elo16* C16 elongase, *Des9*  $\Delta$ -9 desaturase, *Des12*  $\Delta$ -12 desaturase, *Elo9*  $\Delta$ -9 elongase, *Des8*  $\Delta$ -8 desaturase, *Des5*  $\Delta$ -5 desaturase, *Des17*  $\Delta$ -17 desaturase. **b** PKS pathway. *PKS* polyketide synthase.

Variation in the fatty acid content of *Y. lipolytica* YIP56 (**c**), *M. alpina* R807 (**d**), and *Schizochytrium* sp. HX308 (**e**) during fermentation. In (**c**–**e**), the data are presented as the means  $\pm$  s.d. from three ( $n = 3$ ) biologically independent replicates.

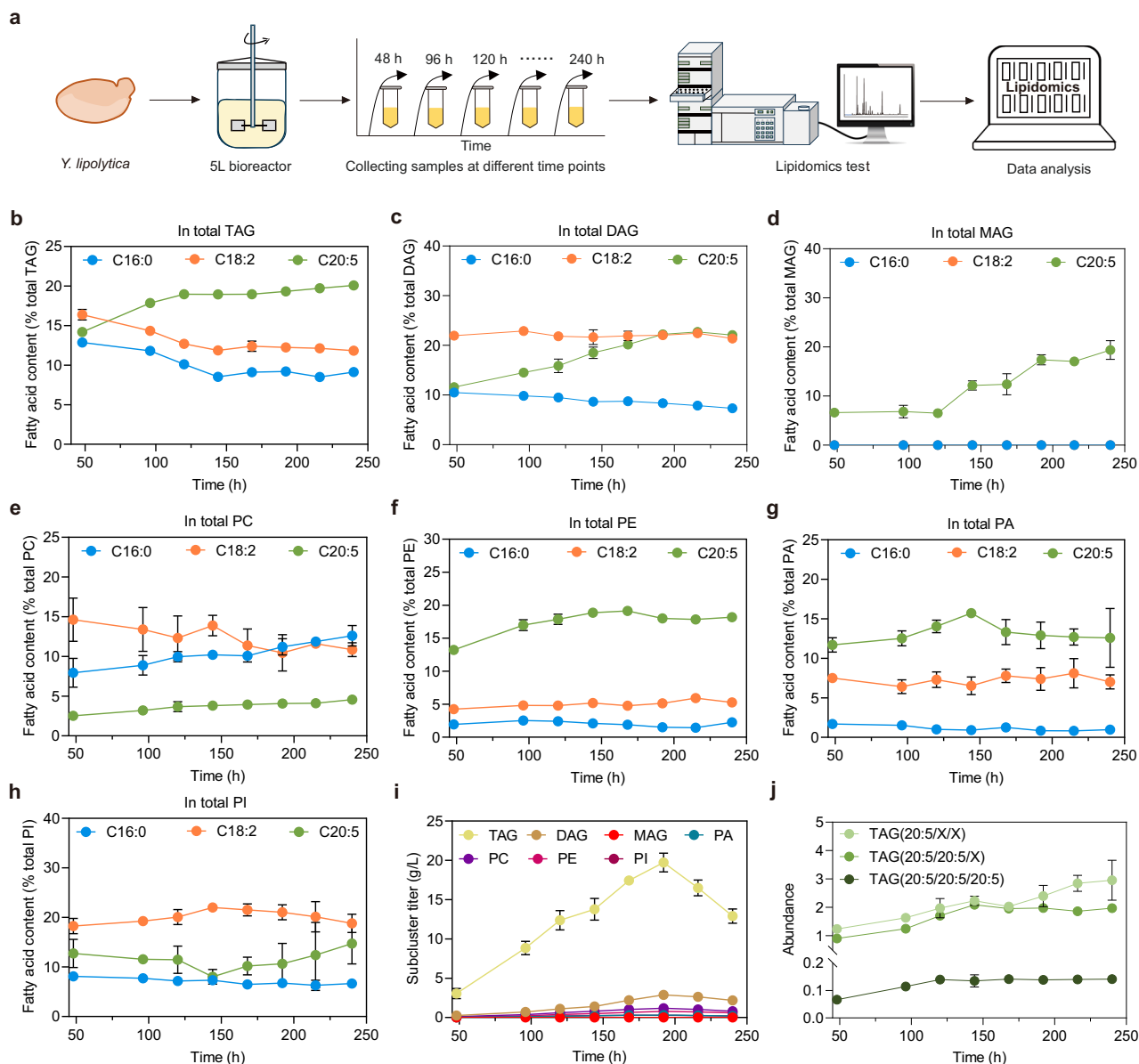


**Fig. 2 | Lipidomic analyses for exploration of the distribution of FAs in different lipid species.** **a** Overall workflow of lipidomic testing. Variation in the fatty acid content of the total TAG (**b**), DAG (**c**), MAG (**d**), PC (**e**), PE (**f**), PA (**g**), and PI (**h**) samples. TAG triacylglycerol, DAG diacylglycerol, MAG monoacylglyceride, PC phosphatidylcholine, PE phosphatidylethanolamine, PA phosphatidic acid, PI

phosphatidylinositol. **i** Variation in the titers of the major lipid species. **j** Abundance of TAG (C20:5/X/X), TAG (C20:5/C20:5/X), and TAG (C20:5/C20:5/C20:5). In (**b–j**), the data are presented as the means  $\pm$  s.d. from three ( $n = 3$ ) biologically independent replicates.

(Supplementary Fig. 2). Although the TAG titer initially increased and then decreased (Fig. 2i), the abundance of TAG (C20:5/X/X), TAG (C20:5/C20:5/X), and TAG (C20:5/C20:5/C20:5) continuously increased (Fig. 2j). These results indicated that the FAs were reshuffled in TAG.

### Verification of the hypotheses contributing to the FA profile changes

Based on FA biosynthesis pathways in *Y. lipolytica* (Fig. 3a), two hypotheses were proposed to explain the mechanism of the continuous increase in C20:5 content, whereas the lipid titer decreased at the later stage of fermentation in *Y. lipolytica* YIP56. Hypothesis 1: More of the original precursor FA (C16:0) was synthesized (Fig. 3b). To verify hypothesis 1, the sole carbon source, glucose, was depleted at 168 h to inhibit C16:0 biosynthesis. The results revealed a large reduction in the C16:0 content, whereas C20:5 still slightly increased after 192 h

(Fig. 3b). In addition, cerulenin, a fatty acid synthesis pathway inhibitor, was added at 168 h to inhibit C16:0 biosynthesis, and the results showed that the content of C16:0 decreased significantly and the content of C20:5 increased slightly (Supplementary Fig. 3); thus, hypothesis 1 was excluded. Hypothesis 2: the transcription levels of the desaturase/elongase pathway were increased in the later stage of fermentation (Fig. 3c). To verify hypothesis 2, the transcription levels of seven genes in the desaturase/elongase pathway were tested at 144, 192, and 240 h. The results revealed that the transcription levels of the seven genes were similar at three time points (Fig. 3c); thus, hypothesis 2 was also excluded.

### Validation of TAG cycling in *Y. lipolytica*

Furthermore, hypothesis 3 was proposed: TAG cycling resulted in a continuous increase in the C20:5 content. TAG cycling is the process of continuous degradation of TAG to release the free FAs that are

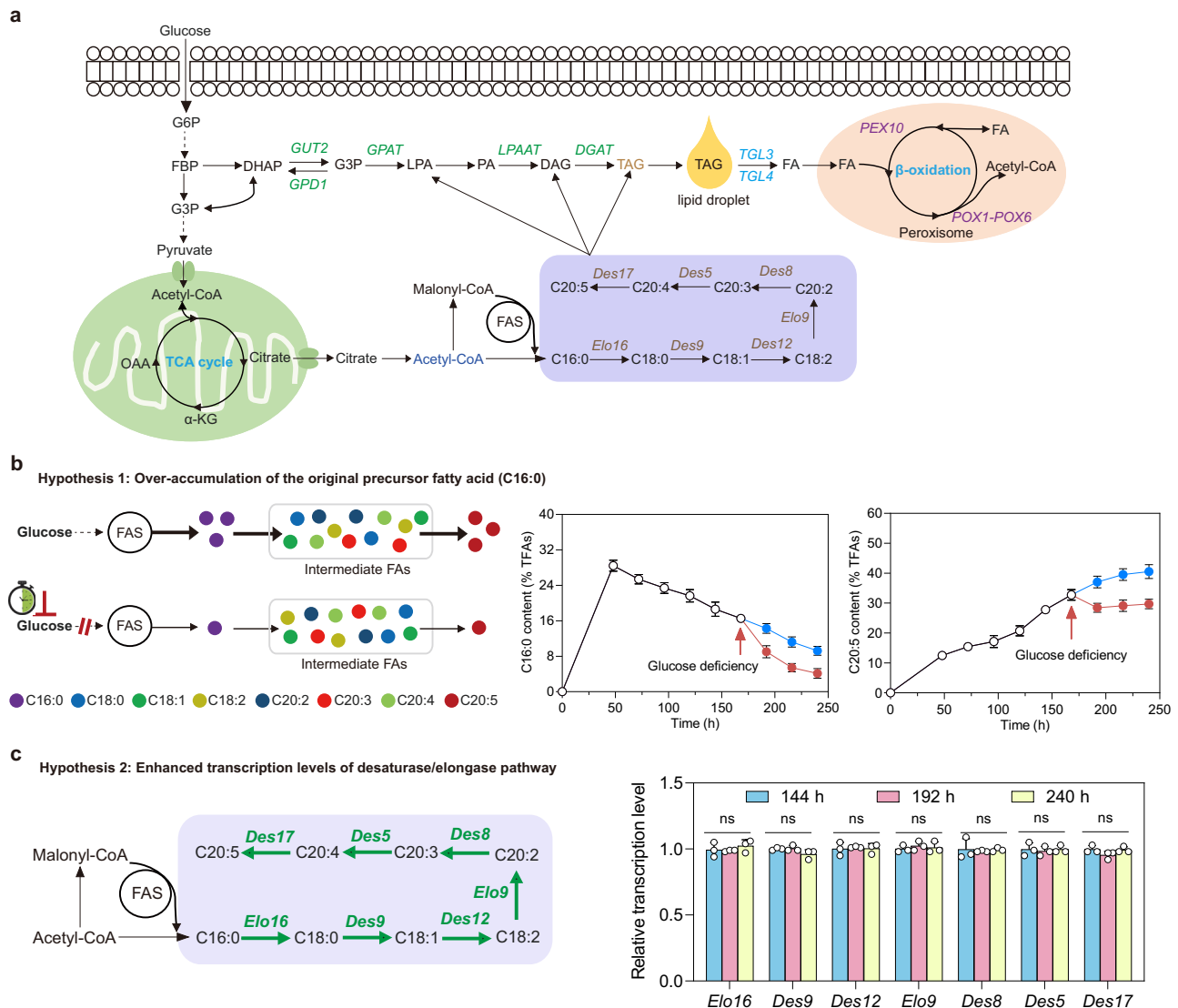


**Fig. 3 | Exploring the effects of precursor overaccumulation and pathway activation on C20:5 synthesis in *Y. lipolytica*.** **a** Schematic of the metabolic pathways related to FA biosynthesis in *Y. lipolytica*. G6P 6-phospho gluconate, FBP fructose biphosphate, G3P glycerol-3-phosphate, OAA oxaloacetate,  $\alpha$ -KG  $\alpha$ -ketoglutarate, FAS fatty acid synthesis, *GUT2* glycerol-3-phosphate dehydrogenase, *GPD1* glycerol-1-phosphate dehydrogenase, *GPAT* glycerol-3-phosphate acyl-transferase, *LPAAT* lysophosphatidate acyl-transferase, *DGAT* diacylglycerol acyl-transferase, *TGL3/TGL4* triacylglycerol lipase, *PEX10* peroxisomal biogenesis factor 10, *POX* peroxisomal acyl-CoA oxidase. **b** Analysis of the effects of C16:0

overaccumulation on the C20:5 biosynthesis. Glucose was removed at 168 h, the red line represents the fatty acid content in the absence of glucose, and the blue line represents the fatty acid content in the presence of glucose. The red arrow represents the time point of glucose deficiency. **c** Analysis of the transcription levels of seven desaturase/elongase genes related to C20:5 biosynthesis at 144, 192, and 240 h. **b, c** Data are presented as the means  $\pm$  s.d. from three ( $n = 3$ ) biologically independent replicates. Statistical analysis was performed using two-tailed Student's *t*-test (\* $P < 0.05$ ).

subsequently used to resynthesize a new FA and enter the re-accumulation of TAG. Specifically, the free FAs, which were produced by the degradation of TAG through lipase, entered the FA pool and were further converted into C20:5 by the desaturase/elongase pathway for the re-accumulation of TAG (Supplementary Fig. 4). To verify hypothesis 3, the inhibition and acceleration of TAG cycling were examined.

To inhibit TAG cycling, two strategies were applied (Fig. 4a). In strategy 1, the key gene responsible for TAG degradation, *TGL4*, was knocked out to yield the engineered strain YIP56- $\Delta$ TGL4; this strategy resulted in less free FAs production. In strategy 2, the key gene responsible for  $\beta$ -oxidation, *PEX10*, was overexpressed to yield the engineered strain YIP56-PEX10; this strategy allowed more free FAs to be degraded to acetyl-CoA rather than enter the desaturase/elongase pathway. Compared with the YIP56 strain, the two engineered strains

presented an apparent reduction in the consumption rate of C16:0 and the biosynthesis rate of C20:5. The C20:5 contents of YIP56- $\Delta$ TGL4 and YIP56-PEX10 were 34.7% and 19.0%, respectively; these values were 14.3% and 53.1% lower than those of the YIP56 strain (Fig. 4b). In addition, compared with that of the YIP56 strain, the lipid titer of YIP56- $\Delta$ TGL4 increased by 53.2% (Supplementary Fig. 5a), whereas that of YIP56-PEX10 did not significantly change (Supplementary Fig. 5b).

To accelerate TAG cycling, two strategies were applied and included overexpressing the *TGL4* gene to construct the engineered strain YIP56-TGL4 (strategy 3) and knocking out the *PEX10* gene to construct the engineered strain YIP56- $\Delta$ PEX10 (strategy 4); these strategies could increase the number of free FAs entering the desaturase/elongase pathway (Fig. 4c). Compared with the YIP56 strain, the two engineered strains had an apparent increase in the consumption rate of C16:0 and the biosynthesis rate of C20:5. The C20:5 contents of

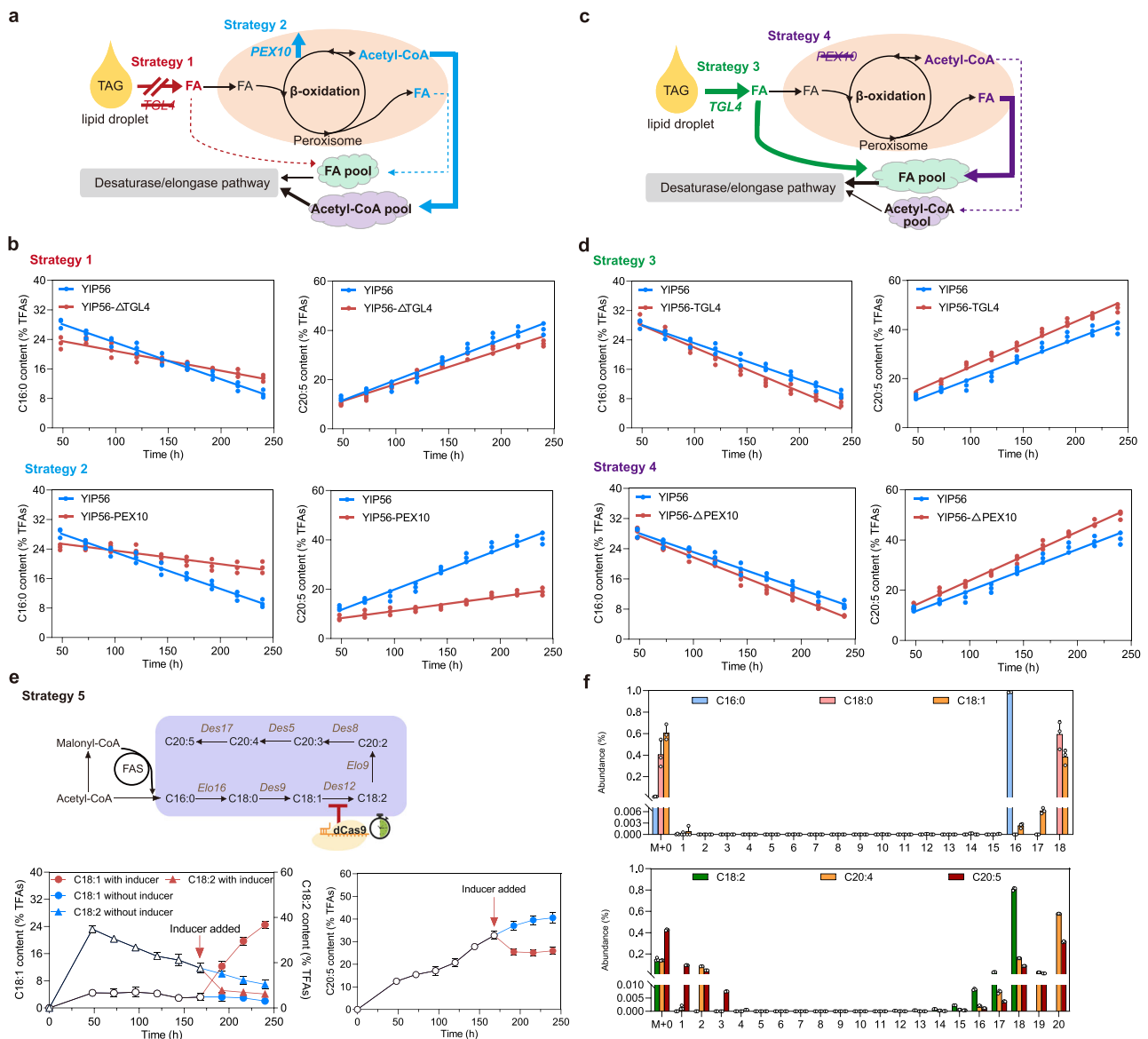


**Fig. 4 | Five strategies used to validate TAG cycling in *Y. lipolytica*.** **a** Description of two strategies used to inhibit TAG cycling. Knocking out the *TGL4* gene (strategy 1, red line) and overexpressing the *PEX10* gene (strategy 2, blue line) decreased the free FA content (dotted line) and increased the acetyl-CoA content (thick line). **b** C16:0 and C20:5 contents of the engineered strains YIP56, YIP56- $\Delta$ TGL4, and YIP56- $\Delta$ PEX10. **c** Description of two strategies to accelerate TAG cycling. Overexpression of the *TGL4* gene (strategy 3, green line) and knockout of the *PEX10* gene (strategy 4, purple line) increased the free FA content (thick line) and decreased the acetyl-CoA content (dotted line). **d** C16:0 and C20:5 contents of the

engineered strains YIP56, YIP56-TGL4, and YIP56- $\Delta$ PEX10. **e** Description of the inhibition of the expression of the *Des12* gene (strategy 5) and the corresponding changes in the C18:1, C18:2, and C20:5 contents. The inducer was added at 168 h, the red line represents the fatty acid content in the presence of the inducer, and the blue line represents the fatty acid content in the absence of the inducer. The red arrow represents the time point of inducer addition. **f** The abundance of  $^{13}$ C-labeled fatty acids. In **(b, d–f)**, the data are the means  $\pm$  s.d. from three ( $n = 3$ ) biologically independent replicates.

YIP56-TGL4 and YIP56- $\Delta$ PEX10 were 48.7% and 49.9%, respectively; these values were 20.2% and 23.2% higher than those of the YIP56 strain (Fig. 4d). In addition, compared with that of the YIP56 strain, the lipid titer of YIP56-TGL4 decreased by 45.0% (Supplementary Fig. 5c), whereas that of YIP56- $\Delta$ PEX10 increased by 23.0% (Supplementary Fig. 5d).

In addition, to explore whether the desaturase/elongase pathway was a key factor for the increase in C20:5 content caused by TAG cycling, we used CRISPRi (under the control of the inducible promoter *P<sub>EYK</sub>*) to inhibit endogenous *Des12* gene expression to block the supply of precursor FAs for C20:5 synthesis (strategy 5) (Fig. 4e). After adding the inducer (erythritol) at 168 h, the content of C18:1 clearly increased,

whereas the content of C18:2 significantly decreased. However, the content of C20:5 moderately increased after 216 h and reached 25.9% (Fig. 4e). Furthermore, to characterize the flow direction of FAs, UL- $^{13}$ C18:2 was used to detect the distribution of FAs containing the  $^{13}$ C labels. The results showed that  $^{13}$ C-labeled carbons were incorporated not only into C20:4 and C20:5 but also into C16:0, C18:0 and 18:1. The relative abundance of M+16 in C16:0 reached 98.6%, and the relative abundances of M+18 in C18:0 and 18:1 reached 59.4% and 38.3%, respectively (Fig. 4f). The results indicated that some products of UL- $^{13}$ C18:2 produced by  $\beta$ -oxidation were used in the biosynthesis of C16:0, C18:0 and C18:1. In summary, TAG cycling was the main reason for the continuous increase in the C20:5 content.



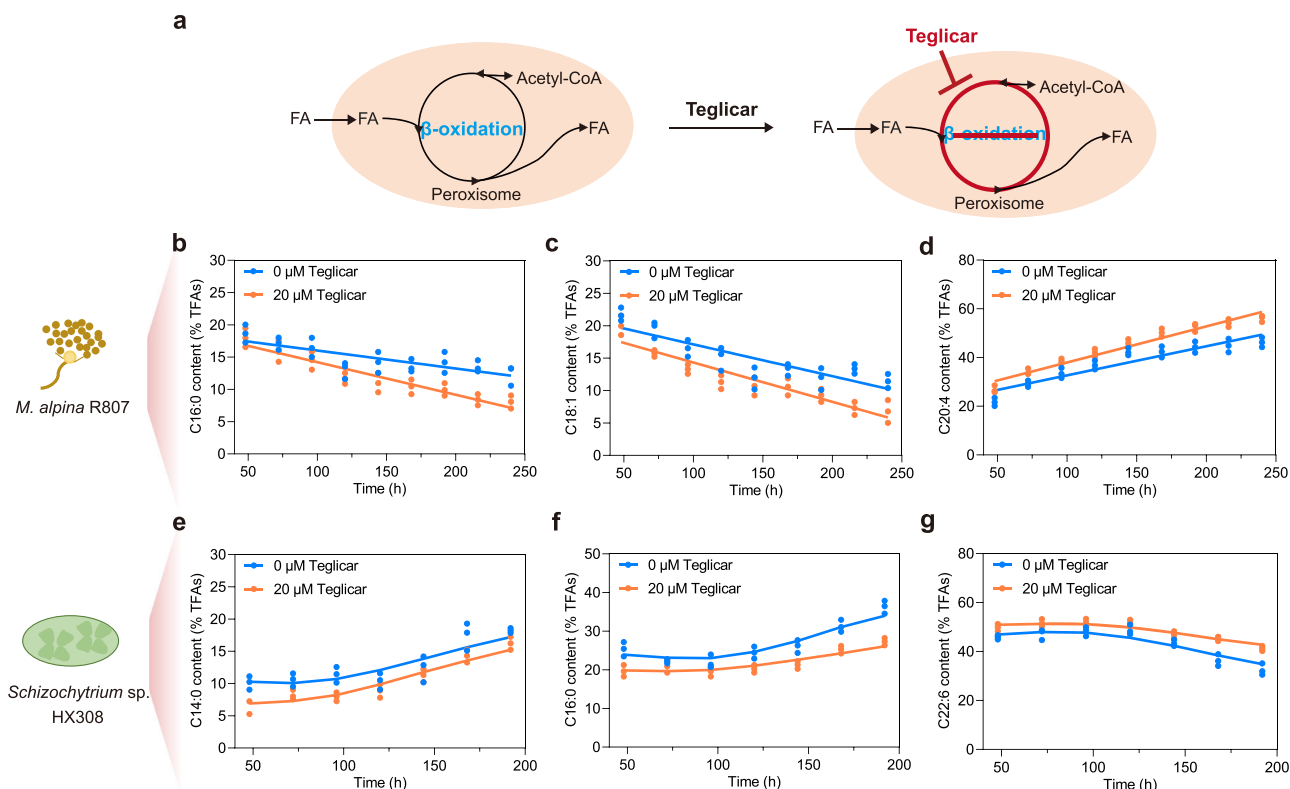


**Fig. 5 | Exploration of the TAG cycling in *M. alpina* and *Schizochytrium* sp.**

**a** Diagram of teglicar inhibition of the  $\beta$ -oxidation pathway. C16:0 content (**b**), C18:1 content (**c**), and C20:4 content (**d**) of *M. alpina* under 0  $\mu$ M and 20  $\mu$ M teglicar.

C14:0 content (**e**), C16:0 content (**f**), and C22:6 content (**g**) of *Schizochytrium* sp.

under 0  $\mu$ M and 20  $\mu$ M teglicar. In (**b–g**), the data are presented as the means  $\pm$  s.d. from three ( $n = 3$ ) biologically independent replicates.

### Exploration of TAG cycling in *M. alpina* and *Schizochytrium* sp.

To verify whether TAG cycling could lead to FA profile changes in *M. alpina* and *Schizochytrium* sp., teglicar, the reversible carnitine palmitoyltransferase 1 was used to accelerate TAG cycling (Fig. 5a). Teglicar has been used to inhibit the  $\beta$ -oxidation pathway in many organisms<sup>21</sup>. By comparing the DCW, lipid titer, and FA profile of the fermentation results with different teglicar concentrations, 20  $\mu$ M teglicar was selected for subsequent experiments (Supplementary Fig. 6a, b). For *M. alpina*, compared with the non-added teglicar group, the consumption rates of C16:0 and C18:1 content in the added group increased, and their contents were lower than the 35.1% and 41.0% of the non-added group at 240 h, respectively (Fig. 5b, c). The synthesis rate of C20:4 in the added group was greater than that in the non-added group, and its content reached 56.1% at 240 h (Fig. 5d). In addition, the lipid titer of the added group significantly increased to 1.48 times greater than that of the non-added group and finally reached 29.8 g/L (Supplementary Fig. 7a). However, in *Schizochytrium* sp., the addition of teglicar did not result in a trend similar to that of *M. alpina*. Compared with those in the non-added group, the contents of C14:0 and C16:0 in the added group decreased and then increased after 120 h and reached 16.2% and 27.3%, respectively (Fig. 5e, f). The content of C22:6 clearly decreased after 120 h, and the final content decreased to 41.3% (Fig. 5g). No significant changes were observed in the lipid titer or DCW in the added group (Supplementary Fig. 7b). C20:4 was synthesized through the desaturase/elongase pathway in *M. alpina*; thus, accelerating TAG cycling could increase the C20:4 content. However, the content of C22:6 could not be increased by accelerating TAG cycling in *Schizochytrium* sp. because C22:6 was synthesized de novo from acetyl-CoA through the PKS pathway.

### Decoupling of TAG synthesis and degradation

In general, the synthesis of TAG from glucose is accompanied by the degradation of TAG. However, TAG synthesis requires nitrogen restriction, and this stress condition accelerates cell senescence and TAG degradation<sup>22</sup>; this results in the PUFA titer initially increasing and then decreasing with prolonged fermentation time (Strategy 1, Fig. 6a). Blocking TAG degradation, such as by knocking out the *TGL4* gene and  $\beta$ -oxidation-related genes, is a common method for increasing PUFA titer<sup>10</sup> (Strategy 2, Fig. 6b). However, blocking TAG degradation has a negative effect on lipid metabolism and energy homeostasis<sup>23</sup>; thus, the PUFA titer cannot be sustainably improved.

Here, based on the TAG cycling, we proposed a strategy in which TAG synthesis and degradation were decoupled to improve the production of PUFAs and their derivatives. This strategy consisted of two stages: in stage I, inhibiting TAG cycling for the overaccumulation of TAG, and in stage II, TAG cycling was accelerated to enhance the desaturase/elongase process of FAs. Specifically, the dCas9-VPR expression cassette under the control of the  $P_{EYK}$ -inducible promoter was integrated into the *Intc* site of the engineered strain YIP56- $\Delta$ PEX10, and the promoter of the *TGL4* gene was also replaced with the  $P_{EYK}$  promoter; yielded the engineered strain YIP56-D3. In stage I of fermentation, the *TGL4* and *dCas9* genes were not expressed without erythritol, TAG was in a high-speed accumulation stage, and TAG cycling was inhibited. When erythritol was added in stage II of fermentation, the *TGL4* gene and *dCas9* gene were activated and expressed, and the TAG degradation rate and TAG cycling accelerated; thus, the PUFA titer was improved (strategy 3, Fig. 6c). These results revealed that the C20:5 content of strain YIP56-D3 (Strategy 3) increased (Supplementary Fig. 8a). Finally, the C20:5 titer of strain YIP56-D3 was 116.2% higher than that of the YIP56 strain and 45.5% higher than that of strain YIP56-D2 (strategy 2) and reached 19.5 g/L (Fig. 6d).

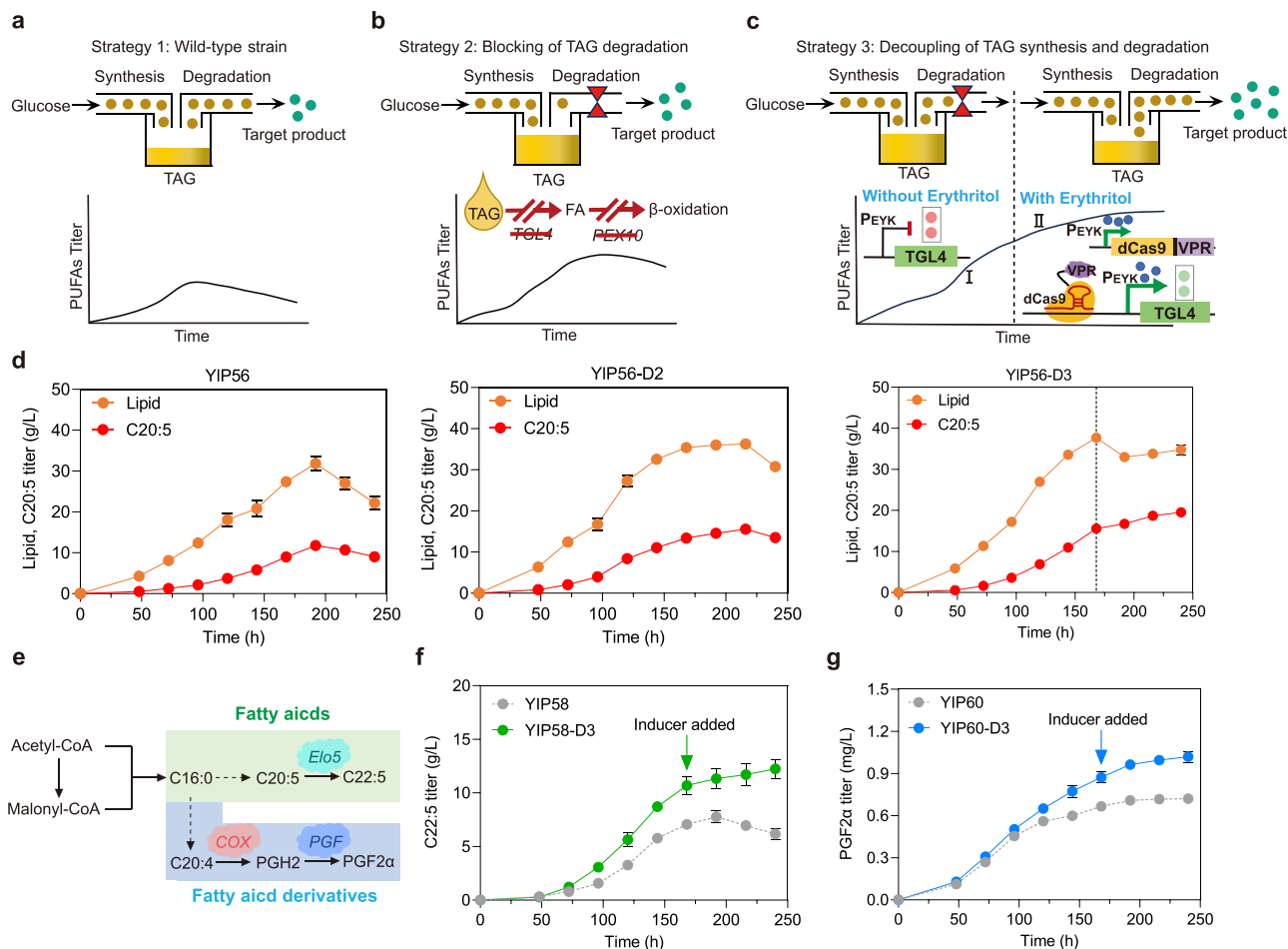


**Fig. 6 | Decoupling the synthesis and degradation of TAG to improve the production of PUFAs and their derivatives.** **a** Diagram of PUFA production in wild-type strains when glucose was used as the initial substrate (Strategy 1). **b** Diagram of PUFA production in the engineered strain after blocking lipid degradation-related genes with glucose as the initial substrate (Strategy 2). Blocking the *TGL4* and *PEX10* genes is represented by red double slash, and TAG degradation process blocking is represented by a red funnel. **c** Diagram of PUFA production in the engineered strain with the decoupling of TAG synthesis and degradation using glucose as the initial substrate. The *TGL4* gene and the *dCas9*-VPR expression cassette are both controlled by the  $P_{EYK}$  promoter. The black dotted line represents the decoupling time point of TAG synthesis and degradation. In stage I of fermentation, the *TGL4* gene is not expressed in the absence of

erythritol (red light). In stage II of fermentation, the *TGL4* and *dCas9* genes are activated and expressed in the presence of erythritol (green light) (Strategy 3). Erythritol is represented by the blue ball. VPR, hybrid tripartite transcriptional activator VP64-p65-Rta. **d** C20:5 and lipid titers of YIP56 and the engineered strains YIP56-D2 and YIP56-D3. The black dotted line represents the decoupling time point of TAG synthesis and degradation. **e** Biosynthesis pathway of C22:5 and PGF2α. *Elo5*,  $\Delta$ -5 elongase; *COX*, cyclooxygenase; *PGF*, prostaglandin F synthase. **f** C22:5 titers of the engineered strains YIP58 and YIP58-D3. The green arrow represents the time point of inducer addition. **g** PGF2α titers of the engineered strains YIP60 and YIP60-D3. The blue arrow represents the time point of inducer addition. In (d, f–g), data are presented as the means  $\pm$  s.d. from three ( $n = 3$ ) biologically independent replicates.

To verify the generality of the strategy, two high-value-added products, C22:5 and PGF2α, were tested. C22:5 is a component of seal oil and plays an important role in cardiovascular and cerebrovascular diseases and body immunity<sup>24</sup>. PGF2α is a C20:4 derivative and has important physiological functions in the digestive, reproductive, and respiratory systems<sup>25</sup>. The *PaC20* gene (encoding  $\Delta$ -5 elongase) was overexpressed in strains YIP56 and YIP56-D3, respectively (Fig. 6e), and the engineered strains YIP58 and YIP58-D3 were obtained. The C22:5 content increased from 26.5% in the YIP58 strain to 38.3% in the YIP58-D3 strain (Supplementary Fig. 8b), and the C22:5 titer reached 12.3 g/L; this value was 1.99 times greater than that of the engineered strain YIP58 (Fig. 6f). The *Des17* gene of strains YIP56 and YIP56-D3 was knocked out by CRISPR, and the codon-optimized *GvCOX* and *MmPGF* genes were integrated into the *Scp2* site of the genome to obtain engineered strains YIP60 and YIP60-D3 (Fig. 6e). The PGF2α titer of YIP60-D3 was 41.7% higher than that of YIP60 and reached 1.02 mg/L (Fig. 6g). The above results indicated that the strategy of decoupling TAG synthesis and degradation could effectively improve the production of PUFAs and their derivatives.

## Discussion

In this work, we have demonstrated the role and mechanism of TAG cycling in PUFA biosynthesis and developed a strategy in which TAG biosynthesis and degradation were decoupled to effectively increase the production of PUFAs and their derivatives.

From the perspective of lipid metabolism, blocking TAG and FA degradation is an efficient strategy for the overproduction of lipids. On the one hand, blocking TAG degradation in yeast, plants, and animals leads to the overaccumulation of lipids<sup>26–28</sup>. In *Saccharomyces cerevisiae*, the *TGL3*, *TGL4*, and *TGL5* genes all encode functional lipases, and their deletion resulted in a 2.49-fold increase in the TAG titer<sup>29,30</sup>. Unlike *S. cerevisiae*, only two genes encoding lipases (*TGL3* and *TGL4*) are found in *Y. lipolytica*. *TGL4* is the main lipase responsible for TAG degradation, and *TGL3* may act as a positive regulator of *TGL4* rather than a functional lipase. Knocking out the *TGL4* gene resulted in a 1.8-fold increase in the lipid titer<sup>31</sup>. In this study, knocking out the *TGL4* gene also resulted in an increase in the lipid titer of 53.1% (Supplementary Fig. 5a). However, the independent deletion of lipase could lead to growth delay since it is important for maintaining lipid

homeostasis; this has been demonstrated in *S. cerevisiae*, *Y. lipolytica* YB-392, and *Phaeodactylum tricornutum*<sup>32–34</sup> and was also consistent with our results (Supplementary Fig. 5a). On the other hand, the  $\beta$ -oxidative degradation of FAs occurred mainly in the peroxisomes of oil-producing microorganisms. Six acyl-CoA oxidases (*POX1*–*POX6*) were the catalytic enzymes for the first reaction of  $\beta$ -oxidation, and their deletion resulted in the complete loss of the  $\beta$ -oxidation function, a 1.6-fold increase of FAs titer, but also and an unbalance in FA metabolism<sup>35–37</sup>. However, each acyl-CoA oxidase has a different chain length preference<sup>38</sup>. For example, knocking out the *POX2* gene independently resulted in a significant decrease in long-chain FAs<sup>39</sup>; in this study, knocking out a single *POX* gene did not meet the TAG cycling acceleration needs. In contrast, the *PEX10* gene encodes proteins responsible for peroxisome biogenesis and is involved in peroxisome formation and proliferation without substrate preference<sup>40</sup>. However, excessive accumulation of free FAs led to cell stress. Some studies have shown that independent deletion of the *PEX10* gene can lead to cell stress, which occurs only in media supplemented with oleic acid<sup>41,42</sup>. In this study, the engineered strain YIP56- $\Delta$ PEX10 was grown in medium with glucose as the sole carbon source, which had no negative effect on cell growth (Supplementary Fig. 5d). Moreover, overexpression of the *TGL4* gene led to excessive accumulation of FAs, resulting in a decrease in DCW (Supplementary Fig. 5c); these results indicated that intracellular FAs were produced mainly by TAG degradation and not de novo synthesis via the fatty acid synthesis pathway.

In many oleaginous microorganisms, such as *M. alpina*, *Cryptococcus podzolicus*, and *Parietochloris incisa*, the lipid titer generally shows a decrease in the later fermentation process<sup>43–46</sup>. Several specific conditions could trigger the degradation of accumulated lipids; these conditions include providing FAs for membrane lipid synthesis during the exponential growth phase or upon exit from starvation conditions or providing metabolic energy via peroxisomal  $\beta$ -oxidation upon nutrient depletion occurs<sup>47</sup>. Although the lipid titer decreased, the PUFA content of continued to increase in some microorganisms. In particular, the C20:4 content rapidly increased throughout the ageing process in *M. alpina*; this represented the ageing stage in which the cells stopped growing but did not die<sup>48,49</sup>. The results of the intracellular metabolomics analysis indicated that the C20:4 content increased at the expense of the degradation of other FAs; this was a similar principle to the accelerated TAG cycling observed in our study. We proposed that regulating TAG cycling to increase PUFA production was applicable to microorganisms harboring the desaturase/elongase pathway. For microorganisms in the PKS pathway, PUFAs were synthesized de novo from acetyl-CoA; thus, the free FAs released by TAG degradation could not be further synthesized into PUFAs. Typically, *Schizochytrium* sp. did not improve PUFA synthesis by regulating TAG cycling (Fig. 5g). Similarly, the C20:4 and C20:5 contents of *Aurantiochytrium limacinum* in the PKS pathway did not increase with prolonged fermentation time<sup>50</sup>. However, in *Nannochloropsis gaditana*, *Phaeodactylum tricornutum*, and *Myrmecia incisa*, which use the desaturase/elongase pathway<sup>51,52</sup>, the PUFA content gradually increased with prolonged fermentation time; the results were also consistent with those from our study (Fig. 1a, b).

In this study, all results confirmed that TAG degradation was not a useless process, and provided an insight for better utilization of TAG degradation in constructing a superior cell factory for lipid production was provided. In the early stage of fermentation, TAG cycling was inhibited to enhance TAG overaccumulation, and TAG cycling was then accelerated to promote PUFAs production in the later stage of fermentation. The titers of C20:5, C22:5, and PGF2 $\alpha$  increased by 116.2%, 99.4%, and 41.7%, respectively. This strategy was applicable only to microorganisms whose FAs are synthesized via the desaturase/elongase pathway. Future advances will focus on comprehensively utilizing TAG degradation to maximize the potential of developing oil-producing microbial cell factories.

## Methods

### Plasmids and strains

In this study, all plasmids were constructed by Gibson assembly. The products (homologous arms, target genes) obtained via polymerase chain reaction (PCR) were digested, recovered, and then ligated to the pUC-HUH vector backbone to overexpress or knock out genes in *Y. lipolytica*. Plasmid pCRISPRi was used as a vector for inhibiting the expression of the *Des12* gene. Plasmid pCRISPRyl was used as a vector for replacing the promoter of *TGL4* and knocking out the *Des17* gene. These constructed plasmids of the pUC series were digested with *EcoR* I and *Not* I to yield the linear portions; these portions were introduced into the starting strain *Y. lipolytica* YIP56 using the chemical transformation method (Frozen-EZ Yeast Transformation II Kit, Zymo Research, Orange, CA).

*Y. lipolytica* YIP56 is an engineered strain that overexpresses  $\Delta$ -8 desaturase,  $\Delta$ -9 elongase,  $\Delta$ -5 desaturase, and  $\Delta$ -17 desaturase (lab stock). The linear portions, pUC-Scp2-TGL4 and pUC-Scp2-PEX10 integrated into the *Scp2* site of *Y. lipolytica* YIP56 by homologous recombination to overexpress *TGL4* and *PEX10*, respectively, and the engineered strains of YIP56-TGL4 and YIP56-PEX10 were obtained. The linear portions, pUC-HUH- $\Delta$ TGL4 and pUC-HUH- $\Delta$ PEX10, were used to knock out *TGL4* and *PEX10* by homologous recombination in isolation or in a combinatorial manner, and the engineered strains of YIP56- $\Delta$ TGL4, YIP56- $\Delta$ PEX10, and YIP56-D2 were obtained. Using YIP56 as the starting strain, the promoter of *TGL4* was replaced with P<sub>EYK</sub>, and the P<sub>EYK</sub>-dCas9-VPR expression cassette was integrated into the *Intc* site to obtain the engineered strain YIP56-D3. The linear portion, pUC-Scp2-PaC20, was integrated into the *Scp2* sites of YIP56 and YIP56-D3 by homologous recombination to produce C22:5, and the engineered strains of YIP58 and YIP58-D3, respectively, were obtained. The linear portions of pUC-Scp2-PGF were integrated into the *Scp2* sites of YIP56 and YIP56-D3 with *Des17* gene deletion by homologous recombination to produce PGF2 $\alpha$ , and the engineered strains of YIP60 and YIP60-D3, respectively, were obtained. The competent cells were coated with SD medium and incubated at 28 °C for 48–60 h. Genomic DNA was the colony PCR template and was extracted using the E.Z.N.A. Yeast DNA Kit (Omega Bio-Tek, Inc.). The URA gene is a screening marker and was used for counterselection on yeast extract peptone dextrose (YPD) solid plates supplemented with 5-fluoroorotic acid (5-FOA) (Macklin, China). The URA-deficient strain could be used as the starting strain for the next transformation.

*M. alpina* R807 and *Schizochytrium* sp. HX308 are industrial PUFA producers. *E. coli* DH5 $\alpha$  was used for recombinant plasmid construction. All plasmids and strains used in this study are provided in Supplementary Tables 1 and 2. All overexpressed genes and promoter sequences used in this study are provided in Supplementary Data 1, and primer sequences used in this study are provided in Supplementary Data 2 (synthesized in Sangon Biotech, China).

### Strain culture conditions

Luria-Bertani (LB) medium (10 g/L tryptone, 5 g/L yeast extract, and 10 g/L NaCl) supplemented with 50 mg/L ampicillin was used for *E. coli* culture unless otherwise noted. *E. coli* was generally cultured at 37 °C for 12–14 h.

YPD medium (20 g/L glucose, 20 g/L peptone, and 10 g/L yeast extract) was used for the culture of *Y. lipolytica*. Synthetic defined (SD) solid medium (5 g/L (NH<sub>4</sub>)<sub>2</sub>SO<sub>4</sub>, 20 g/L glucose, 1.7 g/L yeast nitrogen base (YNB), and 30 g/L agar) was used to screen the *Y. lipolytica* transformants. YPD solid medium supplemented with 5-FOA was used to remove the URA3 counterselection marker. Fermentation medium (2.5 g/L yeast extract, 0.3 g/L peptone, 1.7 g/L YNB without amino acids, and 60 g/L glucose) was used as fermentation medium to produce lipids and C20:5. A single colony of *Y. lipolytica* was inoculated into YPD liquid medium and grown at 220 rpm and 28 °C overnight to obtain the seed mixture.



For *M. alpina*, seed medium I (2 g/L yeast extract, 30 g/L glucose, 2 g/L  $\text{KH}_2\text{PO}_4$ , and 10 g/L corn syrup) and seed medium II (6 g/L yeast extract, 50 g/L glucose, 2 g/L  $\text{KH}_2\text{PO}_4$ , and 4 g/L corn syrup) were used for cell culture. Potato glucose agar (PDA) slanted medium (200 g/L potato, 20 g/L glucose, and 20 g/L agar) was used for slant inoculation. The fermentation medium (10 g/L yeast extract, 80 g/L glucose, 4 g/L  $\text{KH}_2\text{PO}_4$ , 3 g/L  $\text{NaNO}_3$ , and 0.5 g/L  $\text{MgSO}_4 \cdot 7\text{H}_2\text{O}$ ) was used to produce lipids and C20:4 in *M. alpina*. A loop of *M. alpina* mycelia was inoculated on a PDA slant and incubated at 25 °C for 5–7 days. The mycelia were cultured in seed medium I and II in sequence for 20–24 h at 25 °C with shaking at 125 rpm and then inoculated into fermentation medium for lipid production.

For *Schizochytrium* sp., seed medium (20 g/L  $\text{NaSO}_4$ , 4.6 g/L  $\text{MgSO}_4 \cdot 7\text{H}_2\text{O}$ , 4.8 g/L  $(\text{NH}_4)_2\text{SO}_4$ , 1.25 g/L NaCl, 1 g/L KCl, 20 g/L monosodium glutamate, 4 g/L  $\text{KH}_2\text{PO}_4$ , 4 g/L yeast extract, and 50 g/L glucose) was used for cell culture. The fermentation medium (12 g/L  $\text{NaSO}_4$ , 2 g/L  $\text{MgSO}_4 \cdot 7\text{H}_2\text{O}$ , 4 g/L  $(\text{NH}_4)_2\text{SO}_4$ , 0.5 g/L KCl, 0.7 g/L  $\text{K}_2\text{SO}_4$ , 0.15 g/L  $\text{CaCl}_2$ , 20 g/L monosodium glutamate, 4 g/L  $\text{KH}_2\text{PO}_4$ , 4 g/L yeast extract, 100 g/L glucose, 0.008 g/L  $\text{MnCl}_2$ , 0.008 g/L  $\text{ZnSO}_4$ , 0.0001 g/L  $\text{CoCl}_2$ , 0.0001 g/L  $\text{NaMnO}_4$ , 0.006 g/L  $\text{CuSO}_4$ , 0.006 g/L  $\text{NiSO}_4$ , 0.02 g/L  $\text{FeSO}_4$ , 0.2 % (v/v) Vitamin B1, 0.2 % (v/v) Vitamin B6, and 0.2 % (v/v) Vitamin B12) was used to produce lipids and C22:6. *Schizochytrium* sp. was cultured at 170 rpm and 28 °C overnight.

Additionally, the fermentation broths of *M. alpina* and *Schizochytrium* sp. were supplemented with teglicars (MedChemExpress, USA) at different concentrations (5, 10, 20, 30, 40, and 50  $\mu\text{M}$ ) for 72 and 48 h in flasks to test the DCW, lipid titer, and FA profile.

### Lipidomic and $^{13}\text{C}$ metabolic flow analysis

For Lipidomic analysis, during the fed-batch fermentation process of *Y. lipolytica*, 5 mL of 24 samples at eight time points (48, 96, 120, 144, 168, 192, 216, and 240 h,  $n=3$ ) were collected. These 24 samples were centrifuged at  $8000 \times g$  for 2 min to obtain the cells, and the cells were then preserved with liquid nitrogen. Lipidomics analysis was performed at Majorbio (Shanghai): 50 mg samples were homogenized at 50 Hz and  $-10^\circ\text{C}$  for 6 min using a high-throughput tissue crusher WonBio-96C (Shanghai Wonbio Technology Co., Ltd), followed by sonication at 40 kHz and  $5^\circ\text{C}$  for 30 min. Subsequently, the samples were placed at  $-20^\circ\text{C}$  for 30 min, centrifuged at  $13,000 \times g$  at  $4^\circ\text{C}$  for 15 min, and then 350  $\mu\text{L}$  of the lipid extract from the upper phase was transferred to a new tube and evaporated to dryness under a gentle stream of nitrogen. The dry samples were reloaded by brief sonication with 100  $\mu\text{L}$  isopropanol:acetonitrile (1:1, v/v) loading solution in a  $5^\circ\text{C}$  water bath. The extracted lipids were centrifuged at  $13,000 \times g$  for 15 min at  $4^\circ\text{C}$ , and 2  $\mu\text{L}$  of the supernatant was injected into a Thermo UHPLC-Q Exactive HF-X Vanquish Horizon system, equipped with Accucore C30 column (100  $\times$  2.1 mm i.d., 2.6  $\mu\text{m}$ ; Thermo, USA). The mobile phase consisted of solvent A (10 mM ammonium acetate in acetonitrile:  $\text{H}_2\text{O}=1:1$  (v/v) (0.1% (v/v) formic acid)), and solvent B (2 mM ammonium acetate in acetonitrile: isopropanol:  $\text{H}_2\text{O}=10:88:2$  (v/v) (0.02% (v/v) formic acid)). Injection parameters were as follows: volume: 2  $\mu\text{L}$ , flow rate: 0.4 mL/min, column temperature:  $40^\circ\text{C}$ , and total chromatographic separation for 20 min. The solvent gradient of solvent B was varied according to the following conditions: linear gradient from 35% to 60% (0–4 min); from 60% to 85% (4–12 min); from 85% to 100% (12–15 min), 100% standing (15–17 min); from 100% to 35% (18–20 min), and maintained at 35% until the end of separation. The ion-spray voltage floated at  $-3000\text{ V}$  in negative mode and at  $+3000\text{ V}$  in positive mode, and the detection was carried out over a mass range of 200–2000  $m/z$ . After UHPLC-MS/MS analyses, the raw data were imported into the LipidSearch (Thermo, CA) for peak detection, alignment, and identification. Lipidomic features detected in at least 80% of any set of samples were retained. After filtering, minimum metabolite values were imputed for specific samples in which the metabolite levels fell below the lower limit of quantitation and each

metabolic features were normalized by sum. The response intensity of the sample mass spectrum peaks was normalized by the sum normalization method, and the normalized data matrix was obtained for subsequent analysis.

For  $^{13}\text{C}$  metabolic flow analysis, 8 mg of  $\text{UL-}^{13}\text{C}18:2$  (Shanghai Yuanye Bio-Technology Co., Ltd, China) was added at 178 h, and the mixture was cultured for 20 h. Next, 5 mL of fermentation broth was collected and centrifuged at  $8000 \times g$  for 2 min; afterwards, the cells were washed twice with phosphate-buffered saline (PBS). The cells were subsequently preserved with liquid nitrogen. The  $^{13}\text{C}$  metabolic flow was examined at Novogene (Beijing, China).

### Real-time quantitative PCR (RT-qPCR) assay

The total RNA of *Y. lipolytica* YIP56 was extracted using a FastPure Universal Plant Total RNA Isolation Kit (Vazyme, China). Then, the RNA was reverse transcribed into cDNA with HiScript III RT SuperMix (Vazyme, China). cDNA, as a template, and was used for RT-qPCR analysis (QuantStudio™ 3 Real-Time PCR Instrument, 96-well, Thermo, USA). Using the *G6PDH* gene (encoding glucose-6-phosphate dehydrogenase) as an internal reference gene, the relative expression level of the elongase/desaturase gene was determined using the  $2^{-\Delta\Delta\text{CT}}$  method. The primers used for RT-qPCR are provided in the Supplementary Data 2.

### Metabolite extraction and analysis

**Lipid quantification and FA profile analysis:** A total of 20 mg of lyophilized cells was accurately weighed and suspended in 500  $\mu\text{L}$  of sodium hydroxide in methanol (1 mol/L), followed by the addition of 100  $\mu\text{L}$  of internal standard comprising 2 g/L methyl heptadecanoate (Sigma-Aldrich) and 2 g/L glyceryl triheptadecanoate (Sigma-Aldrich) in hexane. The above mixed samples were vortexed at 1200 rpm for 5 h. Then, 40  $\mu\text{L}$  of 98% sulfuric acid was added to neutralize the sodium hydroxide, after which 400  $\mu\text{L}$  of hexane was added, followed by vortexing at 1200 rpm for 30 min to extract the fatty acid methyl esters. The mixed samples were centrifuged at  $8000 \times g$  for 3 min. The upper organic phase was transferred into a glass vial for gas chromatography. The samples were analyzed using a GC-2030 system (Shimadzu, Japan) equipped with a flame ionization detector (FID) and a DB-23 GC column (60.0 m  $\times$  0.25 mm  $\times$  0.25  $\mu\text{m}$ , Agilent, USA). Nitrogen was used as a carrier gas, and its rate was 20 mL/min. The temperatures of the inlet and FID detector were  $250^\circ\text{C}$  and  $280^\circ\text{C}$ , respectively. The column conditions were as follows: initial column temperature of  $100^\circ\text{C}$ , increased to  $196^\circ\text{C}$  at a rate of  $25^\circ\text{C}/\text{min}$ , and then increased using a slower rate of  $2^\circ\text{C}/\text{min}$  to  $220^\circ\text{C}$  and held for 10 min. The detection volume was 1  $\mu\text{L}$ . Each FA methyl ester peak was identified based on its unique retention time. Total lipids and FAs were quantified by comparison with commercial fatty acid methyl ester standards normalized to methyl heptadecanoate and glyceryl triheptadecanoate.

The DCW was determined by gravimetry. A 5 mL culture at different time points was centrifuged at  $8000 \times g$  for 3 min. The supernatant was discarded, and the cells were washed twice with PBS. Then, the cells were lyophilized for 48 h and transferred to pre-weighed filter paper for weight measurement.

**Glucose concentration:** the samples were centrifuged at  $8000 \times g$  for 3 min to collect the supernatant, which was subsequently diluted 100 times with deionized water. Glucose-lactate SBA-40E Biosensory Analyzer (Yanhe, China) was used to test the glucose concentration.

**Prostaglandin assay:** the samples were centrifuged at  $8000 \times g$  for 5 min to collect the cells and supernatant, respectively. The supernatant was diluted 100 times with PBS for detection. The cells were subsequently washed twice with PBS. Next, the cells were broken by repeated grinding with liquid nitrogen. The broken cells were dissolved with PBS and centrifuged to obtain the supernatant, which was subsequently diluted 100 times with PBS for detection. PGF2 $\alpha$  was

measured using General Prostaglandin F2 Alpha (PGF2 $\alpha$ ) ELISA Kit (JonnBio, Shanghai). The PGF2 $\alpha$  concentration was calculated from the standard data diluted to the level within the standard line.

### Fed-batch fermentation

Fed-batch fermentation experiments with *Y. lipolytica* and *Schizochytrium* sp. were performed in 5 L bioreactors (T&J Bioengineering Co., Ltd., Shanghai, China). Fed-batch fermentation experiments with *M. alpina* were performed in a 1000 mL baffled flask.

For *Y. lipolytica*, a single colony was inoculated into 20 mL of YPD liquid medium and grown at 220 rpm and 28 °C overnight. The culture mixture was transferred to 200 mL of YPD liquid medium to obtain a seed culture; this culture was inoculated into 1.5 L fermentation medium at a 10% ratio and cultured for 240 h (0.35 vvm, 28 °C). Unlike shake-flask fermentation, the fermentation medium in bioreactor contained 2.5 g/L yeast extract, 0.3 g/L peptone, 1.7 g/L YNB without amino acids, and 2.7 g/L (NH<sub>4</sub>)<sub>2</sub>SO<sub>4</sub>, and initial glucose concentration was 100 g/L. The agitation speed was varied between 300 and 1000 rpm to maintain the dissolved oxygen concentration above 20% of the atmospheric value. The pH of the culture was constantly controlled at 5.50  $\pm$  0.2 by automatically adding 10 mol/L sodium hydroxide. 800 g/L glucose was fed when the glucose concentration was lower than 30 g/L, and 200 mL ammonium sulfate (17.6 g/L) was fed at a speed of 8 mL/h after 24 h. In addition, 1  $\mu$ g/mL cerulenin (aladdin, China) was added at 168 h to inhibit C16:0 biosynthesis. In the experiment of glucose starvation, the glucose feeding rate was adjusted according to the glucose consumption rate to ensure the glucose concentration in the medium was 0 at 168 h. In the experiment of inhibiting *Des12* gene expression, erythritol (Sangon Biotech, China) was added at 168 h to activate the expression of the *dCas9* gene to inhibit *Des12* gene expression. In the decoupling strategy, 40 g/L erythritol was added at 168 h (the dividing point between Stages I and II of fermentation) to activate and express the *dCas9* and *TGL4* genes.

For *M. alpina*, a loop of mycelia was inoculated on a PDA slant and incubated at 25 °C for ~5–7 days. The mycelia were cultured in seed medium I and II in sequence for 20–24 h at 25 °C with shaking at 125 rpm and then inoculated into 200 mL fermentation medium and cultured for 240 h. Unlike shake-flask fermentation, the initial glucose concentration in bioreactor was 80 g/L, and 800 g/L glucose was supplemented when the residual glucose concentration was lower than 20 g/L. In addition, 20  $\mu$ M teglicar was added to inhibit the  $\beta$ -oxidation of FAs.

For *Schizochytrium* sp., 1 mL of glycerol-preserved cells was inoculated into 100 mL of seed medium and passaged for three generations, and the resulting culture was inoculated into 3 L of fermentation culture at a 10% ratio and cultured for 192 h (0.4 vvm, 28 °C). The initial agitation speed was set at 250 rpm, and the maximum speed reached 450 rpm. The initial glucose concentration was 80 g/L, and 800 g/L glucose was supplemented with a 50 g/L feed rate when the residual glucose concentration was lower than 20 g/L. The pH of the culture was constantly maintained at 6.50  $\pm$  0.2 by automatically adding 3 mol/L NaOH or citric acid. In addition, 20  $\mu$ M teglicar was added to inhibit the  $\beta$ -oxidation of FAs.

Additionally, the FA content, lipid titer, DCW, and residual glucose concentration were measured every 24 h.

### Statistical analysis

All experiments in the study were performed in three biological replicates. The response curves of the FA contents of the three microorganisms were calculated using linear regression or smooth differentiate/integrate curve fitting in GraphPad Prism version 8.0.2 (GraphPad Inc., USA). All results are expressed as the means  $\pm$  standard deviations.

### Reporting summary

Further information on research design is available in the Nature Portfolio Reporting Summary linked to this article.

### Data availability

The lipidomics data reported in this study have been deposited in the OMIX, China National Center for Bioinformation / Beijing Institute of Genomics, Chinese Academy of Sciences (<https://ngdc.cncb.ac.cn/omix>; accession no. OMIX009484). Source data are provided with this paper.

### References

1. Uthandi, S. et al. Microbial biodiesel production from lignocellulosic biomass: new insights and future challenges. *Crit. Rev. Environ. Sci. Technol.* **52**, 2197–2225 (2022).
2. Kim, H. M., Chae, T. U., Choi, S. Y., Kim, W. J. & Lee, S. Y. Engineering of an oleaginous bacterium for the production of fatty acids and fuels. *Nat. Chem. Biol.* **15**, 721–729 (2019).
3. Ye, Z., Xu, Y. J. & Liu, Y. F. Influences of dietary oils and fats, and the accompanied minor content of components on the gut microbiota and gut inflammation: a review. *Trends Food Sci. Technol.* **113**, 255–276 (2021).
4. Worthmann, A. et al. Fatty acid synthesis suppresses dietary polyunsaturated fatty acid use. *Nat. Commun.* **15**, 45 (2024).
5. Gajewski, J., Pavlovic, R., Fischer, M., Boles, E. & Grininger, M. Engineering fungal de novo fatty acid synthesis for short chain fatty acid production. *Nat. Commun.* **8**, 14650 (2017).
6. Zhu, Z. et al. Multidimensional engineering of *Saccharomyces cerevisiae* for efficient synthesis of medium-chain fatty acids. *Nat. Catal.* **3**, 64–74 (2020).
7. Gao, J. et al. Engineering co-utilization of glucose and xylose for chemical overproduction from lignocellulose. *Nat. Chem. Biol.* **19**, 1524–1531 (2023).
8. Lazar, Z., Liu, N. & Stephanopoulos, G. Holistic approaches in lipid production by *Yarrowia lipolytica*. *Trends Biotechnol.* **36**, 1157–1170 (2018).
9. Gray, J. V. et al. “Sleeping beauty”: quiescence in *Saccharomyces cerevisiae*. *Microbiol. Mol. Biol. Rev.* **68**, 187–206 (2004).
10. Lin, L., Ledesma-Amaro, R., Ji, X. J. & Huang, H. Harnessing oleaginous yeast to produce omega fatty acids. *Trends Biotechnol.* **42**, 335–338 (2024).
11. Dulerio, T. & Nicaud, J. M. Involvement of the G3P shuttle and  $\beta$ -oxidation pathway in the control of TAG synthesis and lipid accumulation in *Yarrowia lipolytica*. *Metab. Eng.* **13**, 482–491 (2011).
12. Trentacoste, E. M. et al. Metabolic engineering of lipid catabolism increases microalgal lipid accumulation without compromising growth. *Proc. Natl. Acad. Sci. USA* **110**, 48–53 (2013).
13. Sharma, A. K. & Wolfrum, C. Lipid cycling isn't all futile. *Nat. Metab.* **5**, 540–540 (2023).
14. Prentki, M. & Madiraju, S. R. Glycerolipid/free fatty acid cycle and islet  $\beta$ -cell function in health, obesity and diabetes. *Mol. Cell. Endocrinol.* **353**, 88–100 (2012).
15. Zanghellini, J. et al. Quantitative modeling of triacylglycerol homeostasis in yeast—metabolic requirement for lipolysis to promote membrane lipid synthesis and cellular growth. *FEBS J.* **275**, 52–63 (2008).
16. Kurat, C. F. et al. Obese yeast: triglyceride lipolysis is functionally conserved from mammals to yeast. *J. Biol. Chem.* **281**, 491–500 (2006).
17. Sharma, A. K., Khandelwal, R. & Wolfrum, C. Futile lipid cycling: from biochemistry to physiology. *Nat. Metab.* **6**, 808–824 (2024).
18. Wunderling, K., Zurkovic, J., Zink, F., Kuerschner, L. & Thiele, C. Triglyceride cycling enables modification of stored fatty acids. *Nat. Metab.* **5**, 699–709 (2023).
19. Yan, C. X. et al. Universal and unique strategies for the production of polyunsaturated fatty acids in industrial oleaginous microorganisms. *Biotechnol. Adv.* **70**, 108298 (2024).
20. Chang, G. et al. The relationship of oxygen uptake rate and k(L) a with rheological properties in high cell density cultivation of

- docosahexaenoic acid by *Schizochytrium* sp. S31. *Bioresour. Technol.* **152**, 234–240 (2014).
21. Wunderling, K. et al. Hepatic synthesis of triacylglycerols containing medium-chain fatty acids is dominated by diacylglycerol acyltransferase 1 and efficiently inhibited by etomoxir. *Mol. Metab.* **45**, 101150 (2021).
  22. Sajjadi, B., Chen, W. Y., Raman, A. A. & Ibrahim, S. Microalgae lipid and biomass for biofuel production: a comprehensive review on lipid enhancement strategies and their effects on fatty acid composition. *Renew. Sust. Energy Rev.* **97**, 200–232 (2018).
  23. Sharma, A. K., Khandelwal, R. & Wolfrum, C. Futile cycles: emerging utility from apparent futility. *Cell Metab.* **36**, 1184–1203 (2024).
  24. Röhrig, F. & Schulze, A. The multifaceted roles of fatty acid synthesis in cancer. *Nat. Rev. Cancer* **16**, 732–749 (2016).
  25. Seo, M. J. & Oh, D. K. Prostaglandin synthases: molecular characterization and involvement in prostaglandin biosynthesis. *Prog. Lipid Res.* **66**, 50–68 (2017).
  26. Upreti, B. K., Morrison, E. N., Emery, R. J. N. & Farrow, S. C. Customizing lipids from oleaginous microbes: leveraging exogenous and endogenous approaches. *Trends Biotechnol.* **40**, 482–508 (2022).
  27. Kim, M. J. et al. Gene silencing of Sugar-dependent 1 (JcSDP1), encoding a patatin-domain triacylglycerol lipase, enhances seed oil accumulation in *Jatropha curcas*. *Biotechnol. Biofuels* **8**, 36 (2014).
  28. James, C. N. et al. Disruption of the Arabidopsis CGI-58 homologue produces Chananin-Dorfman-like lipid droplet accumulation in plants. *Proc. Natl. Acad. Sci. USA* **107**, 833–838 (2010).
  29. Athenstaedt, K. & Daum, G. YMR313c/TGL3 encodes a novel triacylglycerol lipase located in lipid particles of *Saccharomyces cerevisiae*. *J. Biol. Chem.* **278**, 317–323 (2003).
  30. Athenstaedt, K. & Daum, G. Tgl4p and Tgl5p, two triacylglycerol lipases of the yeast *Saccharomyces cerevisiae* are localized to lipid particles. *J. Biol. Chem.* **280**, 1–9 (2005).
  31. Dulermo, T. et al. Characterization of the two intracellular lipases of *Y. lipolytica* encoded by TGL3 and TGL4 genes: new insights into the role of intracellular lipases and lipid body organisation. *Biochim. Biophys. Acta* **1831**, 1486–1495 (2013).
  32. Xiu, X. et al. Hyperproduction of 7-dehydrocholesterol by rewiring the post-squalene module in lipid droplets of *Saccharomyces cerevisiae*. *Metab. Eng.* **86**, 147–156 (2024).
  33. Barka, F. et al. Identification of a triacylglycerol lipase in the diatom *Phaeodactylum tricornutum*. *Biochim. Biophys. Acta* **1861**, 239–248 (2016).
  34. Friedlander, J. et al. Engineering of a high lipid producing *Yarrowia lipolytica* strain. *Biotechnol. Biofuels* **9**, 77 (2016).
  35. Ding, L. et al. Peroxisomal  $\beta$ -oxidation acts as a sensor for intracellular fatty acids and regulates lipolysis. *Nat. Metab.* **3**, 1648–1661 (2021).
  36. Leber, C., Polson, B., Fernandez-Moya, R. & Da-Silva, N. A. Overproduction and secretion of free fatty acids through disrupted neutral lipid recycle in *Saccharomyces cerevisiae*. *Metab. Eng.* **28**, 54–62 (2015).
  37. Beopoulos, A. et al. Control of lipid accumulation in the yeast *Yarrowia lipolytica*. *Appl. Environ. Microbiol.* **74**, 79–89 (2008).
  38. Mlícková, K. et al. Lipid accumulation, lipid body formation, and acyl coenzyme A oxidases of the yeast *Yarrowia lipolytica*. *Appl. Environ. Microbiol.* **70**, 918–924 (2004).
  39. Luo, Y. S., Nicaud, J. M., Van-Veldhoven, P. P. & Chardot, T. The acyl-CoA oxidases from the yeast *Yarrowia lipolytica*: characterization of Aox2p. *Arch. Biochem. Biophys.* **407**, 32–38 (2002).
  40. Xue, Z. et al. Production of omega-3 eicosapentaenoic acid by metabolic engineering of *Yarrowia lipolytica*. *Nat. Biotechnol.* **31**, 734–740 (2013).
  41. Dulermo, R., Dulermo, T., Gamboa-Meléndez, H., Thevenieau, F. & Nicaud, J. M. Role of pex11p in lipid homeostasis in *Yarrowia lipolytica*. *Eukaryot. Cell* **14**, 511–525 (2015).
  42. Rutter, C. D. & Rao, C. V. Production of 1-decanol by metabolically engineered *Yarrowia lipolytica*. *Metab. Eng.* **38**, 139–147 (2016).
  43. Qian, X. et al. Co-production of single cell oil and gluconic acid using oleaginous *Cryptococcus podzolicus* DSM 27192. *Biotechnol. Biofuels* **12**, 127 (2019).
  44. Solovchenko, A. E., Khozin-Goldberg, I., Didi-Cohen, S., Cohen, Z. & Merzlyak, M. N. Effects of light intensity and nitrogen starvation on growth, total fatty acids and arachidonic acid in the green microalga *Parietochloris incisa*. *J. Appl. Phycol.* **20**, 245–251 (2008).
  45. Ji, X. J. et al. Efficient arachidonic acid-rich oil production by *Mortierella alpina* through a repeated fed-batch fermentation strategy. *Bioresour. Technol.* **170**, 356–360 (2014).
  46. Bondioli, P. et al. Oil production by the marine microalgae *Nannochloropsis* sp. F&M-M24 and *Tetraselmis suecica* F&M-M33. *Bioresour. Technol.* **114**, 567–572 (2012).
  47. Jeon, Y. G., Kim, Y. Y., Lee, G. & Kim, J. B. Physiological and pathological roles of lipogenesis. *Nat. Metab.* **5**, 735–759 (2023).
  48. Zhang, A. H. et al. Lipid fraction and intracellular metabolite analysis reveal the mechanism of arachidonic acid-rich oil accumulation in the aging process of *Mortierella alpina*. *J. Agric. Food Chem.* **63**, 812–819 (2015).
  49. Yu, Y. et al. Mechanism of arachidonic acid accumulation during aging in *Mortierella alpina*: a large-scale label-free comparative proteomics study. *J. Agric. Food Chem.* **64**, 124–134 (2016).
  50. Ishibashi, Y. et al. PUFA synthase-independent DHA synthesis pathway in *Parietichytrium* sp. and its modification to produce EPA and n-3DPA. *Commun. Biol.* **4**, 1378 (2021).
  51. Ajjawi, I. et al. Lipid production in *Nannochloropsis gaditana* is doubled by decreasing expression of a single transcriptional regulator. *Nat. Biotechnol.* **35**, 647–652 (2017).
  52. Mariam, I. et al. Ameliorating microalgal OMEGA production using omics platforms. *Trends Plant Sci.* **29**, 799–813 (2024).

## Acknowledgements

This work was supported by the Jiangsu Basic Research Center for Synthetic Biology Grant (No. BK20233003 to X.S. and H.H.), the National Natural Science Foundation of China (No. 32422068 to X.S.), the Natural Science Foundation of Jiangsu Province (No. BK20230059 to X.S.), the National Natural Science Foundation of China (No. 22378209 to X.S. and No. 22038007 to H.H.), and the Joint Research Project of Changsanjiao Science and Technology Innovation Community (No. BK20244001 to X.S. and H.H.).

## Author contributions

F.D. conceived the study and wrote the manuscript with assistance from X.S. and H.H. F.D. performed cell cultivation, strain construction, and fermentation regulation of three PUFA producers. X.L. and F.Z. assisted in strain construction and data analysis. Y.H. and D.Z. assisted in strain construction and fed-batch fermentation. W.M. and Q.X. assisted in data analysis and revised the manuscript. All authors contributed ideas and reviewed the manuscript. X.S. supervised and held overall responsibility for the study.

## Competing interests

The authors declare no competing interests.

## Additional information

**Supplementary information** The online version contains supplementary material available at <https://doi.org/10.1038/s41467-025-59599-0>.

**Correspondence** and requests for materials should be addressed to Xiaoman Sun.

**Peer review information** *Nature Communications* thanks the anonymous reviewers for their contribution to the peer review of this work. A peer review file is available.

**Reprints and permissions information** is available at <http://www.nature.com/reprints>

**Publisher's note** Springer Nature remains neutral with regard to jurisdictional claims in published maps and institutional affiliations.

**Open Access** This article is licensed under a Creative Commons Attribution-NonCommercial-NoDerivatives 4.0 International License, which permits any non-commercial use, sharing, distribution and reproduction in any medium or format, as long as you give appropriate credit to the original author(s) and the source, provide a link to the Creative Commons licence, and indicate if you modified the licensed material. You do not have permission under this licence to share adapted material derived from this article or parts of it. The images or other third party material in this article are included in the article's Creative Commons licence, unless indicated otherwise in a credit line to the material. If material is not included in the article's Creative Commons licence and your intended use is not permitted by statutory regulation or exceeds the permitted use, you will need to obtain permission directly from the copyright holder. To view a copy of this licence, visit <http://creativecommons.org/licenses/by-nc-nd/4.0/>.

© The Author(s) 2025